


# Prospects for detecting asteroid-mass primordial black holes in extreme-mass-ratio inspirals with continuous gravitational waves

Andrew L. Miller <sup>1, 2, \*</sup>

<sup>1</sup>*Nikhef – National Institute for Subatomic Physics,  
Science Park 105, 1098 XG Amsterdam, The Netherlands*

<sup>2</sup>*Institute for Gravitational and Subatomic Physics (GRASP),  
Utrecht University, Princetonplein 1, 3584 CC Utrecht, The Netherlands*

(Dated: October 3, 2024)

Despite decades of research, the existence of asteroid-mass primordial black holes (PBHs) remains almost completely unconstrained and thus could still comprise the totality of dark matter (DM). In this paper, we show that standard searches for continuous gravitational waves – long-lived, quasi-monochromatic signals – could detect extreme mass-ratio inspirals of asteroid-mass PBHs in orbit around a stellar-mass companion using future gravitational-wave (GW) data from Einstein Telescope (ET) and the Neutron Star Extreme Matter Observatory (NEMO). We evaluate the robustness of our projected constraints against the eccentricity of the binary, the choice of the mass of the primary object, and the GW frequency range that we analyze. Furthermore, to determine whether there could be ways to detect asteroid-mass PBHs using current GW data, we quantify the impact of changes in current techniques on the sensitivity towards asteroid-mass PBHs. We show that methods that allow for signals with increased and more complicated frequency drifts over time could obtain much more stringent constraints now than those derived from standard techniques, though at slightly larger computational cost, potentially constraining the fraction of DM that certain asteroid-mass PBHs could compose to be less than one with current detectors.

## I. INTRODUCTION

The primordial black hole (PBH) hypothesis may explain a variety of puzzling cosmological observations, including the purported existence of DM [1, 2], LIGO, Virgo and KAGRA binary black hole mergers [3–16], excess microlensing events [17], the missing satellite problem [18], and anisotropies in the cosmic microwave background [19], without introducing physics beyond the standard model [20]. PBHs could have formed from overdensities in the very early in the universe with masses spanning almost 20 orders of magnitude [21]:

$$M_{\text{PBH}} \sim 10^6 M_{\odot} \left( \frac{t}{s} \right), \quad (1)$$

where  $t$  is the time from the Big Bang that PBHs formed. Such a wide mass range motivates the need to consider a variety of PBH formation mechanisms and experiments to detect the presence of such objects.

If PBHs exist, they could compose a fraction or the totality of dark matter (DM). While the fraction of DM that PBHs could compose,  $f_{\text{PBH}}$ , has been heavily constrained across a wide parameter space, one particular regime, asteroid-mass ( $10^{-16} M_{\odot} \lesssim M_{\text{PBH}} \lesssim 10^{-12} M_{\odot}$ ) PBHs, has been able to evade almost all constraints. In this regime, PBHs would be too heavy to avoid evaporating, but too light to amplify the flux from stars that they lens to a high-enough level detectable by microlensing experiments. In particular, if PBHs have masses of

$\lesssim 10^{-10} M_{\odot}$ , their Schwarzschild radii are approximately equal to, or less than, the wavelength of the light that is being lensed [22], resulting in a strong suppression of the amplification induced by the lens [23]<sup>1</sup>.

The inability to obtain constraints in this mass regime motivates the need to consider alternative ways of probing asteroid-mass PBHs.

One promising avenue could be to search for femtolensing of seconds-long gamma ray bursts (GRBs) [28]. In femtolensing, light rays from a GRB would traverse different path-lengths around the PBH lens and thus result in an interference pattern [29]. In particular, a lack of observed femtolensing events of GRBs observed by *Fermi* has led to constraints on  $f_{\text{PBH}} \lesssim 0.1$  between  $\sim [10^{-16}, 10^{-14}] M_{\odot}$  [30], although the assumption of point-mass GRB sources has been questioned: if the GRB source has a finite size, photons would be emitted from different locations on the source, which would all follow different paths as they bend around the lens, potentially masking any oscillations visible in the energy spectrum [29]. Additionally, the large sizes of GRBs relative to the lensing mass in the lensing plane make most unsuitable for such searches, relaxing most projected constraints [31]. Thus, observations of small-size GRBs are needed to produce realistic constraints in the asteroid-mass regime.

Another avenue could be to look at microlensing of

<sup>1</sup> In principle, the Hyper Suprime-Cam (HSC) experiment [24, 25] can probe  $f_{\text{PBH}} \lesssim 1$  for lensing masses down to  $10^{-12} M_{\odot}$  [26], although if the light source has a larger size than assumed in [27], the constraints are almost completely relaxed between  $\sim [10^{-12}, 10^{-11}] M_{\odot}$  [27].

\* andrew.miller@nikhef.nl

light from x-ray pulsars by asteroid-mass PBH lenses, because (1) wave-optics effects are negligible for  $M_{\text{PBH}} \gtrsim 10^{-13} M_{\odot}$  [28], and (2) pulsars are compact objects, which reduces the impact of finite-source size on the lensing of light compared to using extended sources of light [32]. While it is not currently possible to constrain PBHs using RXTE [33], future observations with eXTP [34] may constrain  $f_{\text{PBH}} \lesssim 1$  between  $\sim [\text{few} \times 10^{-16}, \text{few} \times 10^{-13}] M_{\odot}$  [35], reaching at best  $f_{\text{PBH}} \simeq 0.1$  at  $2 \times 10^{-15} M_{\odot}$  (see Fig. 5 of [35]).

Even if eXTP could obtain such constraints in the future, a key mass regime still remains unconstrained that spans almost an order of magnitude,  $\sim [10^{-13}, 10^{-12}] M_{\odot}$ , which lies in between the eXTP and Subaru/HSC constraints. One possible probe of this mass regime lies in attempting to detect GWs from very slowly inspiraling extreme mass-ratio binaries, consisting of an ordinary compact object with a mass  $\mathcal{O}(M_{\odot})$  and a significantly lighter asteroid-mass compact object, i.e. a PBH. Such so-called extreme-mass ratio inspirals (EMRIs) are usually considered in the context of future spaced-based GW detectors, in which an ordinary compact object of  $\mathcal{O}(M_{\odot})$  inspirals around and then plunges into a supermassive black hole [36], though others have considered so-called “mini-EMRI” systems, composed of  $\mathcal{O}(1-10) M_{\odot}$  ordinary compact object with a planetary-mass exotic compact object orbiting around it, that would be visible in current ground-based detectors [37].

We consider solely the inspiral portion of EMRI systems, specifically at frequencies at which the GW signal appears to be almost monochromatic and ever-lasting. Thus, the signal falls into the category of “continuous waves” (CWs), for which extensive method development has taken place over the last few decades within and outside of the LIGO, Virgo and KAGRA collaborations [38–43]. However, by only analyzing the inspiral portion of the lifetime of the EMRI system, we pay a price in sensitivity: while searches for merging black holes reach could reach out to at least Gpc, we could, at best, detect systems at the scale of the Galaxy,  $\mathcal{O}(\text{kpc})$  [44]. Despite the small distance reach of GW searches to such systems, we are still able to project stringent constraints in the asteroid-mass PBH regime.

In this paper, we make a number of considerations regarding the prospects for detection of asteroid-mass PBHs using CW search techniques. While previous works have made specific choices of  $m_1, m_2$  and ignored eccentricity in the context of current CW searches [44, 45], and have not yet been able constrain  $f_{\text{PBH}} \leq 1$ , we now generalize our thinking to see how constraints on the fraction of DM that PBHs could compose change as a function of (1) GW detector choice, (2) CW search parameters ( $T_{\text{FFT}}, \dot{f}_{\text{max}}$ , etc.), (3) source parameters ( $m_1, m_2$ , eccentricity), and (4) GW frequency bands that are analyzed. Our considerations indicate that searches for CWs can make significant contributions to constraining the asteroid-mass PBH regime, especially if some analysis

methods are tuned to consider PBH EMRIs, *and* even if no changes are made to existing analysis methods.

## II. SIGNAL MODEL

Two compact objects in orbit around their center of mass will emit GWs as they approach each other. Equating the orbital energy loss with GW power, we can obtain the rate of change of the frequency over time, i.e. the spin-up  $\dot{f}$ , in the quasi-Newtonian limit (i.e. far from merger) [46]:

$$\begin{aligned} \dot{f}_{\text{gw}} &= \frac{96}{5} \pi^{8/3} \left( \frac{G\mathcal{M}}{c^3} \right)^{5/3} f_{\text{gw}}^{11/3} \equiv k f_{\text{gw}}^{11/3} \\ &\simeq 9.83 \times 10^{-11} \text{ Hz/s} \left( \frac{\mathcal{M}}{10^{-6} M_{\odot}} \right)^{5/3} \left( \frac{f_{\text{gw}}}{50 \text{ Hz}} \right)^{11/3}, \end{aligned} \quad (2)$$

where  $\mathcal{M} \equiv \frac{(m_1 m_2)^{3/5}}{(m_1 + m_2)^{1/5}}$  is the chirp mass of the system,  $f_{\text{gw}}$  is the GW frequency,  $c$  is the speed of light, and  $G$  is Newton’s gravitational constant.

To obtain the signal frequency evolution  $f_{\text{gw}}(t)$  over time, we integrate Eq. (2) with respect to time  $t$ :

$$f_{\text{gw}}(t) = f_0 \left[ 1 - \frac{8}{3} k f_0^{8/3} (t - t_0) \right]^{-\frac{3}{8}}, \quad (3)$$

where  $t_0$  is a reference time for the GW frequency  $f_0$ .

In most of this paper, we consider systems far from merger with sufficiently low  $\mathcal{M} \lesssim 10^{-5} M_{\odot}$ , which means we can binomially expand Eq. (3), which corresponds to  $\dot{f}_{\text{gw}}(t - t_0) \ll f_0$ :

$$f = f_0 + \dot{f}_{\text{gw}}(t - t_0). \quad (4)$$

Our model for GWs from inspiraling systems is thus a sinusoid whose frequency slowly varies over time.

The amplitude  $h_0(t)$  of the GW signal also evolves with time [46]:

$$\begin{aligned} h_0(t) &= \frac{4}{d} \left( \frac{G\mathcal{M}}{c^2} \right)^{5/3} \left( \frac{\pi f_{\text{gw}}(t)}{c} \right)^{2/3} \\ &\simeq 1.61 \times 10^{-25} \left( \frac{1 \text{ pc}}{d} \right) \left( \frac{\mathcal{M}}{10^{-6} M_{\odot}} \right)^{5/3} \left( \frac{f_{\text{gw}}}{50 \text{ Hz}} \right)^{2/3}, \end{aligned} \quad (5)$$

where  $d$  is the luminosity distance to the source.

Inverting Eq. (3), we can also write down an expression for the time the signal spends between two frequencies:

$$\Delta t = -\frac{3}{8} \frac{f_{\text{gw}}^{-8/3} - f_0^{-8/3}}{k}, \quad (6)$$

which, in the limit that  $f_{\text{gw}} \rightarrow f_{\text{isco}}$ , where  $f_{\text{isco}}$  is the frequency at the innermost stable circular orbit (ISCO), and  $f_{\text{isco}} \gg f_0$ , determines the time to merger  $t_{\text{merg}}$

$$\begin{aligned} t_{\text{merg}} &\simeq \frac{5}{256} \left( \frac{1}{\pi f_0} \right)^{8/3} \left( \frac{c^3}{GM} \right)^{5/3} \\ &\simeq 6000 \text{ years} \left( \frac{50 \text{ Hz}}{f_0} \right)^{8/3} \left( \frac{10^{-6} M_{\odot}}{\mathcal{M}} \right)^{5/3}. \end{aligned} \quad (7)$$

### III. SEARCHES FOR CONTINUOUS WAVES

#### A. Background

Multiple groups search for CWs emitted from anywhere in the sky [45, 47]. The parameter space has four dimensions:  $f, \dot{f}, \alpha, \delta$ , where  $\alpha, \delta$  refer to the sky position of the source. Despite such a simplistic signal model, these searches cannot be performed fully coherently, since each sky position has to be targeted individually, and the computational cost of such analyses scales with  $T_{\text{obs}}^6$  [48]. This means that *semi-coherent* CW search techniques must be employed, which divide the data into smaller chunks of length  $T_{\text{FFT}} \ll T_{\text{obs}}$ , in order to both save computational costs ( $\propto T_{\text{obs}}^2 T_{\text{FFT}}^4$  now) and to increase robustness against theoretical uncertainties in the GW search (e.g. phase coherence could be lost over such long observation times). Computational limitations also require that a fixed range of  $\dot{f}$  be searched over, since the number of points in the  $\dot{f}$  grid scales with  $T_{\text{FFT}}^4$  [48].

When searches for CWs do not find a significant candidate, upper limits on the minimum detectable GW amplitude are produced, usually averaged over the sky but not always [45, 49], as a function of frequency. These limits are derived either through injecting fake signals and recovering them with a particular method, or through analytic / data-driven procedures that encapsulate the properties of the noise while producing conservative constraints with respect to those that could have been obtained through injections [45, 50–53]. An example set of sky-averaged synthetic upper limits that we would obtain on the GW amplitude  $h_{0,\text{min}}$  using the ET power spectral density is shown Fig. 1, which will be the starting point for our calculations of projected constraints on PBHs.

#### B. Limitations of current searches and constraints on asteroid-mass PBHs

In practice, when performing an all-sky search, preference is usually given to negative values of  $\dot{f}$ , since the proposed targets of such searches, lumpy isolated neutron stars, should be spinning down, and thus  $|\dot{f}| \lesssim 10^{-9}$  Hz/s. The maximum positive  $\dot{f}$  searched for limits the extent to which we can use Eq. (4) to approximate

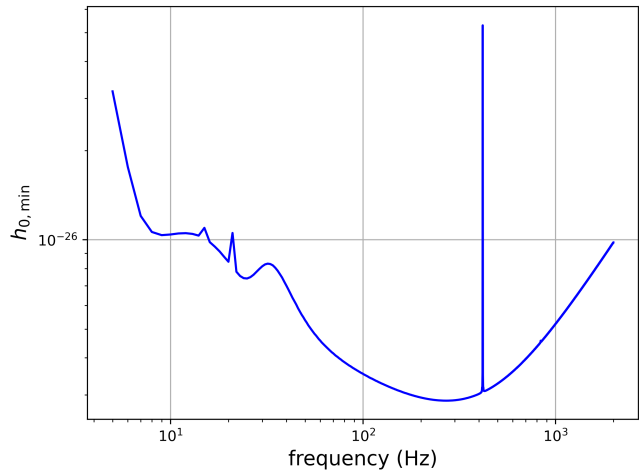


FIG. 1. Synthetic upper limits obtained using Eq. (8) in each 1 Hz band using an ET sensitivity curve and the following analysis parameters:  $T_{\text{FFT}} = 1.5$  days;  $T_{\text{obs}} = 1$  year;  $\Gamma = 0.95$ ,  $CR_{\text{thr}} = 5$ , and  $\theta_{\text{thr}} = 2.5$ .

Eq. (3). Thus, efforts to constrain PBH abundance cannot typically leverage upper limits at frequencies above  $\sim 100$  Hz (see Fig. 1 of [44]), unless  $\mathcal{M}$  is sufficiently small, which, unfortunately, implies smaller  $h_0$  (Eq. (5)). Furthermore, even though in principle PBH abundance for EMRI systems using results from CW searches can be constrained, Refs. [44, 45] do not yet account for eccentricity of such binaries, and how that would impact the constraints, which we will do in Section VI.

### IV. METHODOLOGY

Following [44, 54, 55], we compute the sensitivity to inspiraling PBH binaries obtainable with semi-coherent techniques. In our case, we use a formula to compute the sensitivity of the *frequency-Hough* (a pattern recognition technique used in all-sky searches [56]) towards quasi-monochromatic sources that are sinusoidal within each  $T_{\text{FFT}}$ :

$$\begin{aligned} h_{0,\text{min}} &\simeq \Lambda \sqrt{\frac{S_n(f_{\text{gw}})}{T_{\text{FFT}}^{1/2} T_{\text{obs}}^{1/2}}} \\ &\simeq 5.37 \times 10^{-27} \left( \frac{1.5 \text{ days}}{T_{\text{FFT}}} \right)^{1/4} \left( \frac{1 \text{ year}}{T_{\text{obs}}} \right)^{1/4} \\ &\quad \times \left( \frac{S_n(f_{\text{gw}} = 50 \text{ Hz})}{3.58 \times 10^{-49} \text{ Hz}^{-1}} \right)^{1/2} \left( \frac{\Lambda}{12.81} \right) \end{aligned} \quad (8)$$

where  $\Lambda = 12.81$  for reasonable choices of analysis parameters for the *frequency-Hough* (see Appendix A).

Combining Eq. (8) and Eq. (5), we can obtain an expression for the luminosity distance reach to PBH inspirals:

$$\begin{aligned}
d(f) &= \frac{1}{\Lambda} \sqrt{\frac{T_{\text{FFT}}^{1/2} T_{\text{obs}}^{1/2}}{S_n(f)}} \left( \frac{G\mathcal{M}}{c^2} \right)^{5/3} \left( \frac{\pi f_{\text{gw}}(t)}{c} \right)^{2/3} \\
&\simeq 30 \text{ pc} \left( \frac{1.5 \text{ days}}{T_{\text{FFT}}} \right)^{-1/4} \left( \frac{1 \text{ year}}{T_{\text{obs}}} \right)^{-1/4} \\
&\times \left( \frac{S_n(f = 50 \text{ Hz})}{3.58 \times 10^{-49} \text{ Hz}^{-1}} \right)^{-1/2} \left( \frac{\Lambda}{12.81} \right)^{-1} \\
&\times \left( \frac{\mathcal{M}}{10^{-6} M_\odot} \right)^{5/3} \left( \frac{f_{\text{gw}}}{50 \text{ Hz}} \right)^{2/3} \quad (9)
\end{aligned}$$

After computing the luminosity distance reach, we can write down the space-time volume  $\langle VT \rangle$ :

$$\langle VT \rangle = \frac{4}{3} \pi d(f_{\text{gw}})^3 T, \quad (10)$$

where the brackets indicate the expectation value of the space-time volume. One part of this equation is the Euclidean volume of a sphere, since we do not need to consider any cosmological effects for nearby sources. The other piece,  $T$ , is:  $T = \max(T_{\text{obs}}, \Delta T)$ .  $\Delta T$  is the time spent by the binary system in a given frequency range  $[f, f + \delta f]$ :

$$\begin{aligned}
\Delta T &= \frac{5}{256} \pi^{-8/3} \left( \frac{c^3}{G\mathcal{M}} \right)^{5/3} \left[ f_{\text{gw}}^{-8/3} - (f_{\text{gw}} + \delta f)^{-8/3} \right] \\
&\approx 310 \text{ years} \left( \frac{10^{-6} M_\odot}{\mathcal{M}} \right)^{5/3} \left( \frac{\delta f}{1 \text{ Hz}} \right) \left( \frac{f_{\text{gw}}}{50 \text{ Hz}} \right)^{-11/3} \quad (11)
\end{aligned}$$

where  $\delta f$  is the spacing in frequency at which we evaluate  $d(f)$ . Note that we consider this formulation of  $T$  because the source durations tend to greatly exceed the observation time, so we are sensitive, in one particular frequency bin, to multiple sources emitting GWs before and/or during  $T_{\text{obs}}$  [44, 55]. Now, the number of binaries detectable at a given frequency is:

$$N_{\text{bin}} = \langle VT \rangle \mathcal{R}, \quad (12)$$

where  $\mathcal{R}$  is the formation rate density of binary PBHs. Summing over all possible binaries detected at each frequency

$$N_{\text{bin}}^{\text{tot}} = \sum_i N_{\text{bin}}(f_i). \quad (13)$$

and solving for  $\mathcal{R}$ , assuming no detection ( $N_{\text{bin}}^{\text{tot}} < 1$ ), we arrive at

$$\mathcal{R} = \frac{3}{4\pi} \left( \sum_i \langle VT \rangle (f_i) \right)^{-1}. \quad (14)$$

We can equate the rate densities in Eq. (14) to analytic models for formation rate densities of PBHs in the case of asymmetric-mass ratio binaries, with  $m_2 \ll m_1$ :

$$\begin{aligned}
\mathcal{R} &= 5.28 \times 10^{-7} \text{ kpc}^{-3} \text{ yr}^{-1} f_{\text{sup}} f(m_1) f(m_2) \\
&\times \left( \frac{m_1}{M_\odot} \right)^{-32/37} \left( \frac{m_2}{m_1} \right)^{-34/37} (f_{\text{PBH}})^{53/37}, \quad (15)
\end{aligned}$$

where  $f_{\text{sup}}$  is suppression factor induced by the presence of nearby PBHs that could break up binaries, and  $f(m_1)$  and  $f(m_2)$  are the mass functions of the primary and secondary components of the binary, respectively.

To remain agnostic against particular PBH mass functions and possible rate suppression factors  $f_{\text{sup}}$ , we quote all constraints in terms of an effective fraction  $\tilde{f}$ :

$$\tilde{f} \equiv f_{\text{PBH}} [f_{\text{sup}} f(m_1) f(m_2)]^{37/53}, \quad (16)$$

It is important to note that CW searches will be sensitive only to  $\mathcal{M}$ , which is a particular combination of  $m_1$  and  $m_2$ . Thus, when we interpret synthetic upper limits in terms of constraints on  $\tilde{f}$ , we are free to pick  $m_2$  to be in the asteroid-mass range as long as  $m_1$  is sufficiently heavy to obtain the same  $\mathcal{M}$ . Of course, such EMRI systems may have high eccentricities, which we consider as well in the following sections.

## V. PROJECTED CONSTRAINTS

ET will provide unprecedented low-frequency sensitivity to GWs, enabling us to see much longer signals arising from the inspirals of two compact objects than currently possible with LIGO, Virgo and KAGRA. Furthermore, the sensitivity across all frequencies will increase by approximately an order of magnitude, enabling numerous detections of binary black hole and binary neutron star mergers [57, 58].

It is thus worth asking to what extent ET will be able to detect asteroid-mass PBHs that could form in a binary system. Following the methodology outlined in Section IV, and considering a range of possible EMRI systems, we compute the expected luminosity distance reach and constraints on  $\tilde{f}$ , as shown in Fig. 2(a). We have selected the maximum distance reach possible for each system to plot here, that is, selecting the particular frequency at which the distance reach is maximum. Additionally, we have assumed  $\dot{f}_{\text{max}} < 10^{-9} \text{ Hz/s}$ , which was used in [45], and a frequency evolution given by Eq. (4). Though we make these plots in terms of  $m_1$  and  $m_2$ , the distance reach depends primarily on  $\mathcal{M}$ , which is constant along the diagonal lines in these plots. When computing  $\tilde{f}$ , however, we use the contributions for EMRI systems inspiraling at *all* frequencies, not just the maximum one, as implied by Eq. (14). We evaluate the impact of the range of frequencies chosen on the  $\tilde{f}$  constraint in Section VI.

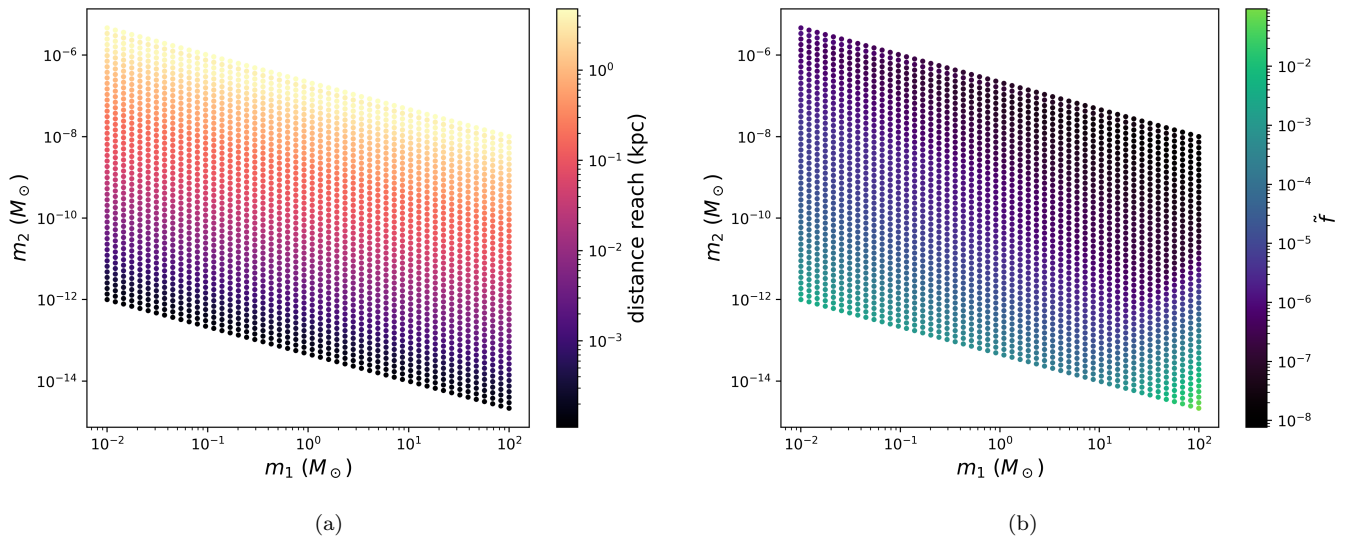


FIG. 2. Using Eq. (9) and the ET power spectral density curve, we have computed the expected luminosity distance reach (left) and  $\tilde{f}$  (right) as a function of  $m_1$  and  $m_2$ , enforcing the criteria that  $\dot{f} \leq \dot{f}_{\max} = 10^{-9}$  Hz/s and that the linear approximation in Eq. (4) holds. We have only plotted points in which  $\tilde{f} < 1$ , and have assumed that the eccentricity is negligible, an assumption that will be relaxed later in Section VI.

## VI. ANALYSIS CONSIDERATIONS

Here, we consider what changes current and future CW analyses could make to enhance their sensitivity to asteroid-mass PBHs.

### A. Varying $\dot{f}_{\max}$

A major limitation of CW searches to probe asteroid-mass PBHs is the linear signal model (Eq. (11)) and the  $\dot{f}_{\max}$  considered. These two criteria are linked: systems with chirp masses above a critical value will require us to use second- or third-order terms in Eq. (4) to model them correctly. Furthermore, even among systems that do follow Eq. (4),  $\dot{f}_{\max}$  prevents higher frequencies from contributing to the sum in Eq. (14), which, as we will argue, degrades the constraint on  $\tilde{f}$ .

We thus ask the question: if CW searches retain the signal model in Eq. (4) but could increase  $\dot{f}_{\max}$ , how would the ability to constrain  $\tilde{f}$  change in ET? We provide an answer to this question in Fig. 3. These plots show that for  $10^{-9}$  Hz/s  $\leq \dot{f}_{\max} \leq 10^{-7}$  Hz/s does not alter the sensitivity much, since the linearity condition in Eq. (4) is violated. Thus, if we remove both the linearity condition and  $\dot{f}_{\max}$ , which would, in practice, require asteroid-mass PBHs to be searched for with different methods [59–61], we find orders of magnitude improvement in the constraint on  $\tilde{f}$ . We will evaluate the suitability of these different methods to probe asteroid-mass PBHs in Section VID.

### B. Impact of eccentricity

Since we are considering binary black holes with such extreme mass ratios, we should evaluate to what extent our results are valid if these systems are eccentric. To begin, we evaluate the impact of eccentricity on the PN0  $\dot{f}$  term (Eq. (2)) [46]:

$$\dot{f}_{\text{ecc}} = \dot{f}_{\text{gw}} g(\epsilon) \quad (17)$$

$$g(\epsilon) = (1 - \epsilon^2)^{-7/2} \left( 1 + \frac{73}{24} \epsilon^2 + \frac{37}{96} \epsilon^4 \right) \quad (18)$$

where  $g(\epsilon)$  is a function arising from considering GW emission in a quasi-elliptical orbit of two masses, and  $\epsilon$  is the eccentricity of the system.

In contrast to matched filtering, CW methods do not require phase coherence across the signal duration, but only within each  $T_{\text{FFT}}$ . Thus, if the spin-up induced by the eccentricity does not shift the signal frequency by more than one frequency bin in each  $T_{\text{FFT}}$ , CW methods would be sensitive to eccentric systems up to some value of eccentricity. In other words, we need to ensure the following condition is met

$$\dot{f}_{\text{ecc}} T_{\text{FFT}} \leq \frac{1}{T_{\text{FFT}}} \quad (19)$$

so that Eq. (4) is valid across the whole  $T_{\text{obs}}$ .

How eccentric inspiraling systems are depends on how they formed [62–64]. Additionally, only limited models exist for eccentricity evolution as a function of time [65].

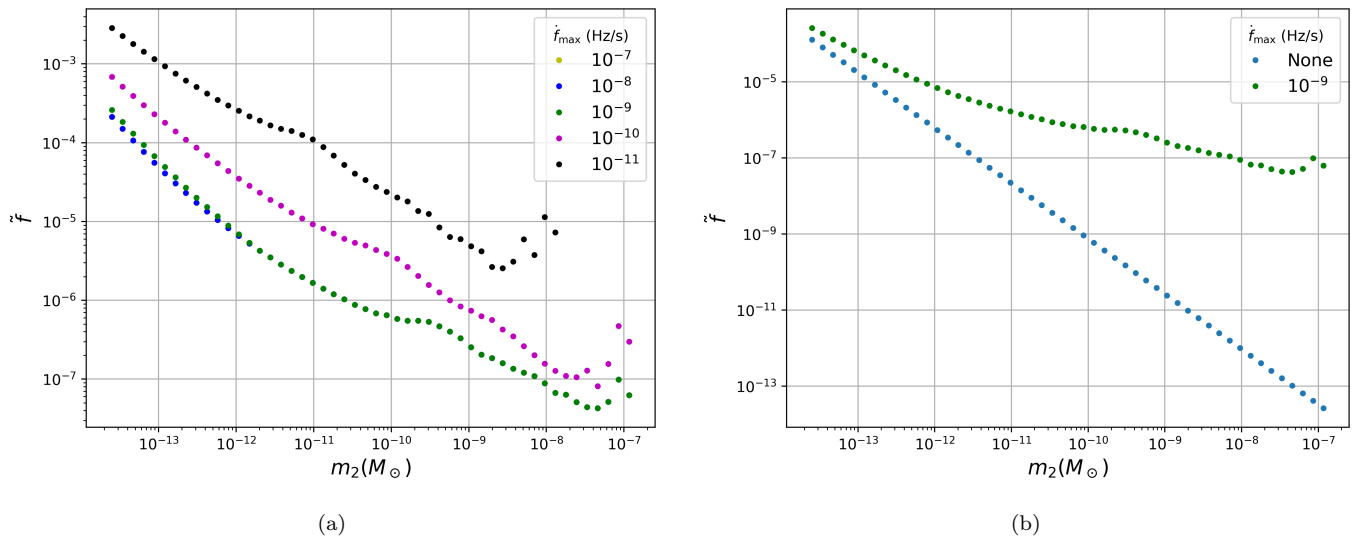


FIG. 3. Left: Varying the maximum spin-up to which CW searches are sensitive results in different constraints on  $\tilde{f}$ . Current searches consider  $\dot{f}_{\max} = 10^{-9}$  Hz/s. We can see that smaller  $\tilde{f}$  indicates not only a poorer sensitivity at small  $m_2$ , but also cannot reach higher values of  $m_2$ , since the signal will spin up to values higher than  $\dot{f}_{\max}$  during  $T_{\text{obs}}$ . The degradation in sensitivity of smaller  $\dot{f}_{\max}$  occurs because signals at higher frequencies cannot contribute to the sum in Eq. (14), since the signal would either take on  $\dot{f} \geq \dot{f}_{\max}$ , and/or the GW frequency evolution cannot be described by Eq. (4) anymore. Right: A comparison showing how much the constraints would improve if no  $\dot{f}_{\max}$  existed, that is, if the signal could be searched for at arbitrarily high  $\tilde{f}$  with a frequency evolution following Eq. (3). In both plots, we have set  $\delta f = 1$  Hz, which represents the approximate spacing in upper limits that is obtained through injections in CW searches [45].

We thus assume the “worst-case” scenario in which the eccentricity is constant throughout the orbit, thus causing the maximum shift in  $\tilde{f}$ . In Fig. 4, we show the impact of eccentricity on the projected constraints for  $\tilde{f}$  for  $m_1 = 2.5M_\odot$  using the ET sensitivity curve. We follow the procedure outlined in Section IV to obtain the distance reached and thus the constraint on  $\tilde{f}$ .

In Fig. 4, we notice that as the eccentricity increases, the maximum  $m_2$  probable with CW methods decreases. This is because  $f_{\text{ecc}}$  becomes too large and thus the condition in Eq. (19) is no longer satisfied. Furthermore, we see a general weakening of the constraint on  $\tilde{f}$  as we increase eccentricity, since the systems with higher frequencies no longer contribute to the sum because the condition in Eq. (19) is more easily violated at high frequencies even though it is met at low frequencies.

### C. From which frequencies does the sensitivity come?

Ironically, the restrictions on linearity in current CW searches imply that lower-frequency signals will always contribute to the sum, but they do not comprise a large gain in sensitivity with respect to those at high frequencies, thus motivating the need to attempt to detect signals at high frequencies and removing restrictions on  $\dot{f}_{\max}$  and linearity. We thus study specifically which dis-

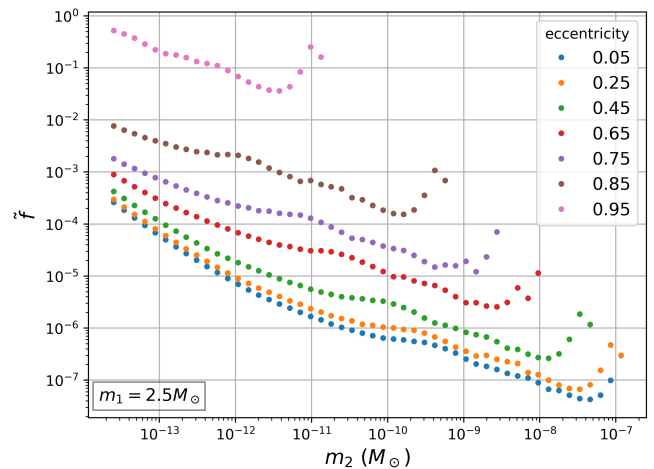


FIG. 4. ET. We vary the eccentricity and compute the expected constraint on  $\tilde{f}$  for a fixed  $m_1 = 2.5M_\odot$ . Highly eccentric systems are much harder to constrain with standard CW searches.

tance reaches, indexed by the GW frequencies in the sum in Eq. (14), contribute the most to the rate density constraint. We show in Fig. 5(a) constraints on the rate density for particular choices of  $m_1$  and  $m_2$ , assuming negligible eccentricity, a linear frequency evolution (Eq. (4))



and  $\dot{f}_{\max} = 10^{-9}$  Hz/s. The way to interpret this plot is as follows: at a given frequency, the sum over distance reaches is taken from that frequency to the maximum one in the plot. For example, for the red curve, at  $f_{\min} \simeq 200$  Hz, we sum the distance reaches from  $f_{\min} \simeq 200$  Hz to  $f_{\max} = 800$  Hz. We notice immediately in the red curve that going to frequencies below 200 Hz does not improve the constraint on the rate density, indicating that the constraint on  $\dot{f}$  does not get better by looking at lower GW frequencies. We can see this behavior in each of the curves on this plot, except that the “cut-off” frequency below which it is no longer is useful to sum the distance reaches in Eq. (14) decreases. This occurs because as  $m_2$  increases, for a fixed  $m_1$ ,  $\mathcal{M}$  increases and thus  $\dot{f}$  increases, indicating that, for higher frequencies, the GW frequency evolution will deviate from Eq. (4). We can see that for the highest value of  $m_2$ , that summing the distance reaches at all available frequencies is immensely helpful. Additionally, Fig. 5(b) shows the frequency range  $[f_{\min}, f_{\max}]$  necessary to analyze to obtain 99% of the sensitivity on the rate density value, as a function of  $m_2$ . This plot is consistent with Fig. 5(a), showing that for smaller values of  $m_2$ , higher frequencies provide the best sensitivity.

#### D. Changes to current CW searches

Based on the discussion in Section VIC, higher frequencies provide most of the constraining power on the rate density and  $\dot{f}$ . In Section VIA, we found that increasing  $\dot{f}_{\max}$  relative to that which is used currently ( $\dot{f}_{\max} = 10^{-9}$  Hz/s) and searching for signals that evolve linearly does not alter the projected constraint on  $\dot{f}$  (Fig. 3(a)), but relaxing the linearity condition could provide orders of magnitude tightening of the constraints on  $\dot{f}$  (Fig. 3(b)). We thus ask to what extent *current* CW searches could constrain asteroid-mass PBHs if these conditions on  $\dot{f}_{\max}$  and linearity are loosened, and what kinds of methods would be necessary to actually search for these systems.

As an example of what could be achieved in the previous observing run of advanced LIGO, Virgo and KAGRA (O3), we show in Fig. 6 how the constraints on  $\dot{f}$  in [45] would change if  $\dot{f}_{\max} = 10^{-9}$  Hz/s were increased and if the linearity condition in Eq. (4) were relaxed. In [45],  $\delta f = \dot{f}_{\max} T_{\text{obs}}^2$ , so the spacing in the O3 interpolated upper limits changes when computing  $\dot{f}$  changes as a function of  $\dot{f}_{\max}$ . Allowing  $\dot{f}_{\max} \rightarrow 100\dot{f}_{\max}$  results in weaker constraints on  $\dot{f}$  than both the magenta and blue curves at certain masses. This occurs because, as shown in Appendix B, there is a non-trivial dependence of  $\dot{f}$  on

the spacing in frequency  $\delta f$  in the case of a flat power spectral density, in which larger  $\delta f$  implies worse limits. However, the actual dependence of  $\dot{f}$  on  $\delta f$ , i.e. when including a frequency-dependent power spectral density and conditions on linearity and  $\dot{f}_{\max}$ , result in a complicated behavior of these constraints, shown in Fig. 6.

Fig. 6 implies that, even now, constraints of  $\dot{f} \lesssim 1$  could be obtained at masses below  $\sim 10^{-10} M_{\odot}$ ; however, relaxing the requirement in Eq. (4) and allowing  $100\dot{f}_{\max} = 10^{-7}$  Hz/s has implications for the computational cost of the search. Increasing  $\dot{f}_{\max}$  would imply an increase in the size of the grid in  $\dot{f}$  that is analyzed in CW searches. Currently, the step-size in  $\delta \dot{f} = 1/(T_{\text{FFT}} T_{\text{obs}}) \sim 3 \times 10^{-11}$  Hz/s at high frequencies [45], where  $T_{\text{FFT}} = 1024$  s. To extend the positive  $\dot{f}$  coverage to  $\dot{f}_{\max} = 10^{-8}$  Hz/s and  $\dot{f}_{\max} = 10^{-7}$  Hz/s would require 3300 and 33000 points more to search over, respectively, which is a 10x to 100x increase in the the number of points in the current spin-down grid, which are  $\sim 320$  negative values and  $\sim 32$  positive ones, at each sky position. Such an increase in computational cost is not currently feasible, since all-sky CW searches already take  $10^7$  CPU core-hours [45, 53], and would not lead to a powerful constraint on  $\dot{f}$  at current detector sensitivity *unless* the linearity condition was relaxed, which would, again, imply increased computational cost to consider  $\dot{f}$  or  $\dot{f}$  terms in Eq. (4). However, searching at a specific point in the sky, e.g. the Galactic Center, would be feasible, since the current “directed” searches towards particular sky positions have orders of magnitude less computational cost than the all-sky ones, since the Doppler shift induced by the relative motion of the earth with respect to the source can be corrected for before doing the analysis [66].

It is thus worth asking if other methods could be used to achieve the constraints given by the black curve now, that is to search for signals that do not strictly follow Eq. (4). Such methods, which are termed tCW methods, search directly for Eq. (3), and thus are sensitive to arbitrarily high values of  $\dot{f}$ .

As an example, we evaluate the computational cost of the Generalized frequency-Hough, a particular tCW method that finds curves in the time-frequency plane [53, 59, 67], at a fixed sky position, for  $T_{\text{FFT}} = 8192$  s. In this method, a grid in  $k$ , instead of  $\dot{f}$ , is constructed, and the loop over each point in this grid constitutes the greatest computational cost of the search.

The spacing in the grid  $dk$  in our case is [67]:

$$dk \approx \frac{11}{3} \left( \frac{k}{T_{\text{FFT}} f_{\text{gw}}} \right) \quad (20)$$

and varies between  $[k_{\min}, k_{\max}]$ , where  $k_{\min} = \dot{f}_{\min}/f_{\max}$  and  $k_{\max} = \dot{f}_{\max}/f_{\min}$ . The number of points in the  $k$  grid is therefore a function of both the specified  $f$  and  $\dot{f}$  range. Furthermore, instead of frequency, there is another grid that has spacing  $dx$ :

<sup>2</sup> This choice implies that, at each frequency at which an upper limit is set, that the signal frequency cannot vary by more than  $\delta f$  over the course of  $T_{\text{obs}}$ .

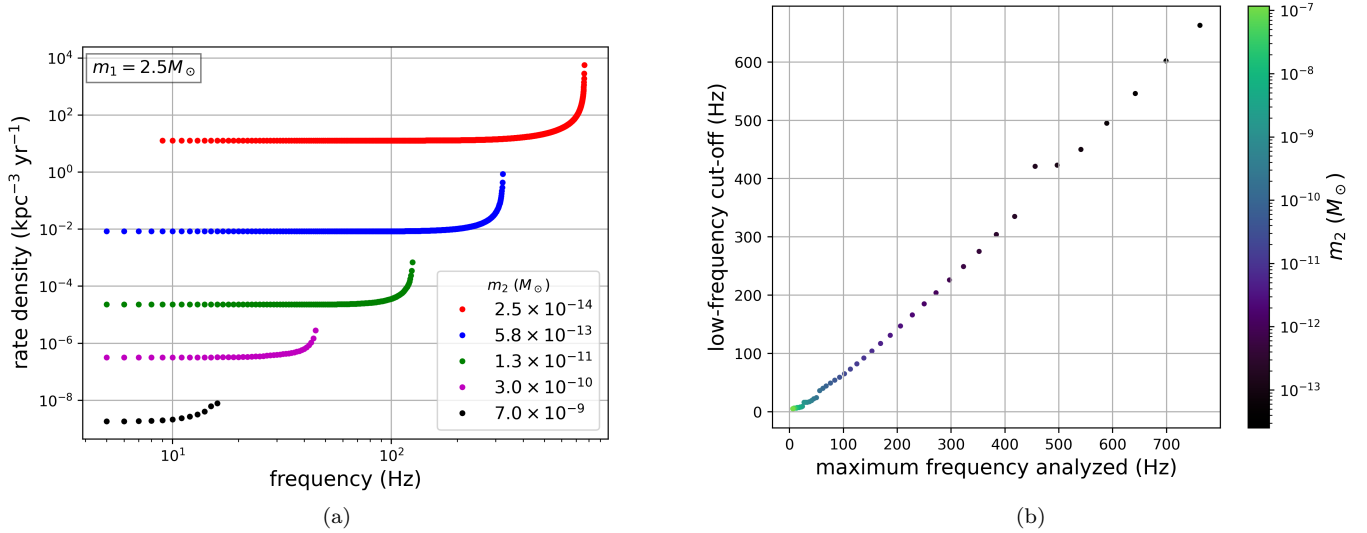


FIG. 5. ET sensitivity curve.  $m_1 = 2.5 M_\odot$ . Left: Accumulated rate density constraint as a function at which frequency we begin to sum the distance reaches in Eq. (14) up to a maximum given by the right-most frequency on each curve. Right: the frequency band to analyze to obtain 99% of the optimal rate density constraint as a function of  $m_2$ , where the “optimal” constraint would arise if we sum distance reaches over the full frequency range.

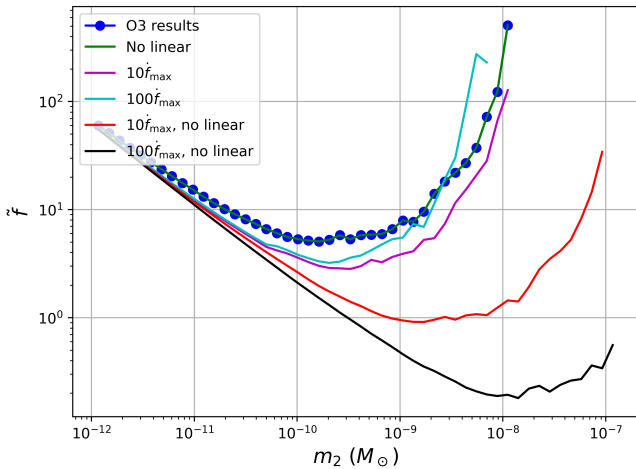


FIG. 6. How the constraint on  $\tilde{f}$  obtained in [45] would change if various conditions of CW searches were relaxed.

$$dx = \frac{8}{3} \frac{1}{T_{\text{FFT}} f_{\text{gw}}^{11/3}} \quad (21)$$

which ranges from  $x_{\text{min}} = 1/f_{\text{max}}^{8/3}$  and  $x_{\text{max}} = 1/f_{\text{min}}^{8/3}$ .

In Fig. 7, we show how the number of points in each grid changes as a function of each 5-Hz frequency band analyzed. In total, knowing that each  $x/k$  point takes about  $50 \mu\text{s}$  [59] to evaluate with the *Generalized frequency-Hough* (though this time is likely to decrease

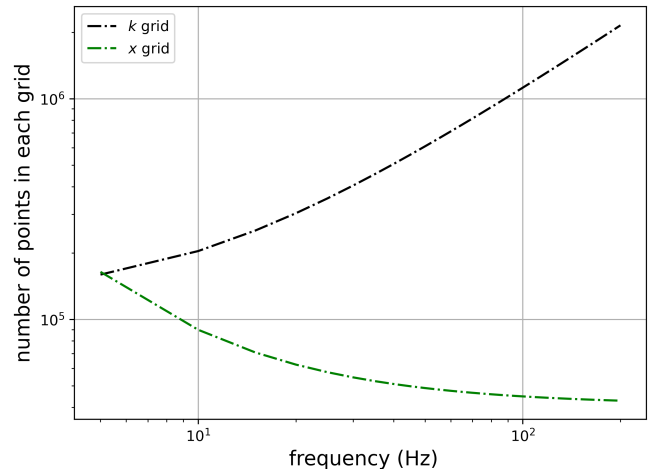


FIG. 7. The number of points in the two grids,  $x$  and  $k$ , that relate to  $f_{\text{gw}}$  and  $\tilde{f}$ , respectively, that would be required to search over using the *Generalized frequency-Hough*. We consider frequency bands of 5 Hz, a spin-up range of  $[10^{-9}, 10^{-7}]$  Hz/s, and  $T_{\text{FFT}} = 8192$  s [45], since we restrict ourselves low frequencies ( $< 100$  Hz) to facilitate direct comparisons with Fig. 5 and because the computational cost increases with  $f_{\text{gw}}$ .

by an order of magnitude or even more<sup>3</sup>), we calculate that a search using the *Generalized frequency-Hough* at one sky position would take  $\sim 2.8 \times 10^4$  core-hours on one

<sup>3</sup> Private correspondence with Lorenzo Pierini



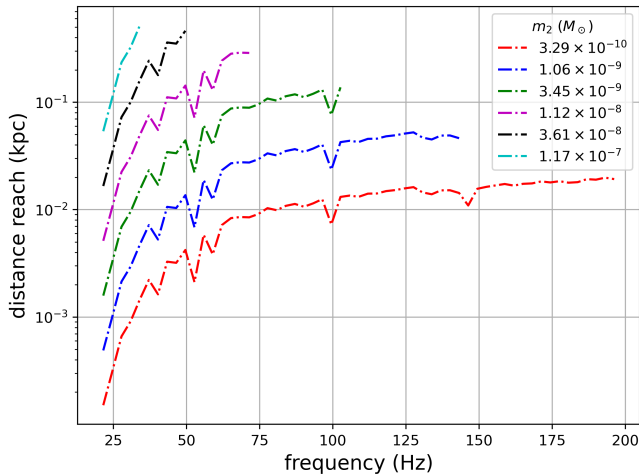


FIG. 8. Distance reach as a function of frequency for the “ $\tilde{f} = 100\hat{f}_{\max}$ , no linear approximation” case shown in Fig. 6 (solid black curve in that figure), restricted to showing a few values of  $m_2$  (different colors) for which  $\tilde{f} \lesssim 1$  in O3.

Quad-Core Intel Core i7. Such a search of one sky position is orders of magnitude cheaper than those presented in [45].

We can also evaluate how many sky points,  $N_{\text{sky}}$ , would be present at low frequencies in order to actually perform an “all-sky search” for such asteroid-mass PBH systems using data from current detectors. Here, we focus  $f_{\text{gw}} < 200$  because for the values of  $m_2$  in Fig. 6 at which we would hope to have a constraint on  $\tilde{f}$  in current detector data, these low frequencies contribute the most to the sum in Eq. (14), as shown in Fig. 8 and demonstrated earlier in Fig. 5(b), and because  $N_{\text{sky}}$  scales with the square of the frequency and  $T_{\text{FFT}}$ :

$$N_{\text{sky}} \simeq 4\pi T_{\text{FFT}}^2 f^2 \frac{v_{\text{orb}}^2}{c^2} \quad (22)$$

where  $v_{\text{orb}}$  is the velocity of earth around the solar-system barycenter. We plot the number of sky points as a function of frequency in Fig. 9 for  $T_{\text{FFT}} = 8192$  s and for  $T_{\text{FFT}} = 1.5$  days. With the expected improvement in the *Generalized frequency-Hough* of about a factor of 10, searching up to  $\sim 200$  Hz would require  $\sim 2.8 \times 10^8$  core-hours, which is a little more than current all-sky searches up to 2048 Hz cost. If we decrease the maximum frequency range to, say, 100 Hz, we would obtain roughly a factor of  $\sim 3 - 4$  decrease in computational cost, and still be sensitive to asteroid-mass PBHs.

## VII. SENSITIVITY OF NEMO TO ASTEROID-MASS PBHS

High-frequency gravitational-wave (HFGW) detectors may deliver exquisite sensitivity in frequency ranges cur-

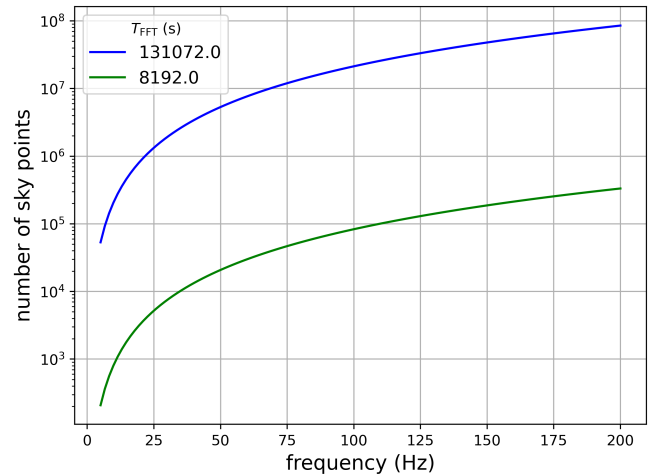


FIG. 9. Number of sky points as a function of GW frequency for two choices of  $T_{\text{FFT}}$ . The green curve corresponds to the  $T_{\text{FFT}}$  used in current all-sky searches for CWs, while the blue curve is drawn with a much longer  $T_{\text{FFT}}$  that we expect to use in the ET era.

rently lacking by current and proposed ground-based detectors [68]. In terms of inspiraling PBHs, at such frequencies, the system will be extremely close to merger, and thus the purely CW approach discussed in Section III would break down. However, searches for “transient CWs” have been shown to be able to track rapid frequency variations of such inspiraling systems over time [52–54, 59–61], and even in the case of “mini-EMRI” systems [37]. While such searches, and also matched filtering ones, have not yet evolved to handle completely eccentric waveforms, it is worth considering how well such EMRI systems could be constrained in future HFGW detectors, in order to motivate the further development of these techniques.

NEMO is a planned high-frequency GW detector that plans to deliver exquisite sensitivity in the 2-4 kHz regime to increase the detection prospects of neutron star mergers, and is comparable to the sensitivities of ET and Cosmic Explorer. For our purposes, however, such high-frequency sensitivity simply implies that we could detect PBH inspirals that are closer to merger than those we have considered in Section V.

Assuming a rough power spectral density value of  $S_n(f) = 10^{-48}$  strain/Hz and a frequency range of [1000,2500] Hz, we calculate the constraint on  $\tilde{f}$  that would arise from a future analysis of NEMO data. We compute the projected constraints following the formalism presented in Section IV; however, because the GW signals become more transient-like and less CW-like as  $m_2$  increases, we actually compute the distance reach using Eq. 32 in [59]. Unfortunately, we only achieve  $\tilde{f} \lesssim 1$  for  $m_2 \gtrsim 10^{-8} M_{\odot}$  – see Fig. 10(a). Thus, we also compute the projected sensitivity assuming that we can use matched filtering. In this case, we calculate compute the

luminosity distance reached following [46]:

$$d = \frac{2}{5} \sqrt{\frac{5}{6}} \frac{c}{\pi^{2/3}} \left( \frac{GM}{c^3} \right)^{5/6} \left( \int_{f_{\min}}^{f_{\max}} df \frac{f^{-7/3}}{S_n(f)} \right)^{1/2} \rho \quad (23)$$

which, when evaluated in the case of  $S_n(f) \sim \text{constant}$ :

$$d \simeq 3.87 \text{ kpc} \left( \frac{8}{\rho} \right) \left( \frac{\mathcal{M}}{10^{-5} M_\odot} \right)^{5/6} \left( \frac{1000 \text{ Hz}}{f_{\min}} \right)^{2/3} \times \left( \frac{1 - (f_{\min}/f_{\max})^{4/3}}{7.053 \times 10^{-1}} \right) \left( \frac{10^{-48} \text{ Hz}^{-1}}{S_n(f)} \right) \quad (24)$$

In Fig. 10(b), we show this projected constraint for different choices of  $m_1$ . In the  $m_1 = 0.1 M_\odot$  curve, we observe a “kink” around  $m_2 \simeq 10^{-10} M_\odot$ , which indicates a sort-of transition between when the signal duration exceeds the observation time, and when the signal becomes more “transient-like”. In practical terms, summing the contributions to the rate densities from different frequencies, outlined in Section IV, does not produce as competitive constraints as simply calculating the rate density in the Euclidean way:

$$\mathcal{R} = \frac{3.0}{\langle VT \rangle} \quad (25)$$

$$\langle VT \rangle = \frac{4}{3} \pi d_{\max}^3 T_{\text{obs}}, \quad (26)$$

where  $d_{\max} = \max_f [d(f)]$  and represents the system with a given  $\mathcal{M}$  sweeping from  $f_{\min}$  to  $f_{\max}$  with a duration given by Eq. (6):  $\Delta t < T_{\text{obs}}$ , i.e. a “transient-like” signal, not a CW.

### VIII. CONCLUSIONS

In this paper, we have shown that CW and tCW searches could constrain the existence of asteroid-mass PBHs in EMRI systems currently and with future GW detectors. In the mass regime in which our projected constraints overlap with those from microlensing, our results provide complementary ways of probing PBHs that could have formed in binary systems, instead of isolated ones. Additionally, in the so-called “asteroid-mass” regime, our results indicate that GW detectors would provide the first-ever stringent constraints on the fraction of DM that PBHs could compose. We note that we have parameterized our constraints in terms of  $\tilde{f}$  in order to remain model-agnostic, and therefore in order to directly and fairly compare with the  $f_{\text{PBH}}$  limits that arise from microlensing experiments or theoretical considerations, we would have to know exactly which assumptions are made on the PBH mass functions and formation mechanisms.

In addition to providing projected constraints, we have evaluated how these constraints would change if we allow the binaries to take on nonzero eccentricities, if we

change the maximum  $\tilde{f}$  up to which is searched, and if we relax the requirement that the GW signal be quasi-monochromatic. Our results show that eccentricity plays a major role in affecting our constraints, and that incorporating it into an analysis may be necessary to achieve the best possible constraints. Furthermore, we determine which GW frequencies we should analyze as a function of the PBH mass  $m_2$  in order to determine where most of the constraining power lies. We find that higher-frequencies for very small  $m_2$  values contains most of the constraining power, while lower frequencies are necessary for heavier  $m_2$ , since the requirement on  $\tilde{f}_{\max}$  prohibits higher frequencies from contributing to the sum in Eq. (14). This study has implications for all-sky searches for PBH inspirals: in fact, we could envision a search in which higher frequencies are prioritized for smaller systems, while lower frequencies are analyzed for heavier ones, instead of blindly searching for all systems at all frequencies. Such a scheme could reduce the computational burden of an all-sky search for PBH inspirals.

Our results show that CW search techniques, exactly as they are, could provide stringent constraints on  $\tilde{f}$  in the ET (3G) era of GW detectors. Furthermore, if tCW methods are used now, they could provide tight constraints on  $\tilde{f}$  using O3 and subsequent observing runs of advanced LIGO, Virgo and KAGRA, highlighting both the short-term and long-term impact of CW searches for asteroid-mass PBHs.

### Appendix A: Additional equations

We provide here more information about Eq. (8), in particular the parameter  $\Lambda$  that encapsulates particular analysis choices made in a real search for quasi-monochromatic GWs. It can be written as [56]

$$\Lambda = 4.02 \left( \frac{p_0(1-p_0)}{\theta_{\text{thr}}^2 p_1^2} \right)^{1/4} \times \sqrt{CR_{\text{thr}} - \sqrt{2} \text{erfc}^{-1}(2\Gamma)}$$

$$p_0 = e^{-\theta_{\text{thr}}} - e^{-2\theta_{\text{thr}}} + \frac{1}{3} e^{-3\theta_{\text{thr}}}$$

$$p_1 = e^{-\theta_{\text{thr}}} - 2e^{-2\theta_{\text{thr}}} + e^{-3\theta_{\text{thr}}} \quad (A1)$$

where, typically,  $\theta_{\text{thr}}$  is the threshold to determine which time-frequency pixels in the equalized power spectrogram are important,  $\Gamma$  is the chosen confidence level, and  $CR_{\text{thr}}$  is a threshold on a detection statistic called the critical ratio, which corresponds to the number of standard deviations a particular outlier is away from the mean. When  $\theta_{\text{thr}} = 2.5$ ,  $\Gamma = 0.95$  and  $CR_{\text{thr}} = 5$ ,  $\Lambda = 12.81$ .

### Appendix B: Dependence of constraints on $\delta f$

We mentioned that the constraint on  $\tilde{f}$  has some dependence on the choice we make for  $\delta f$  in the context

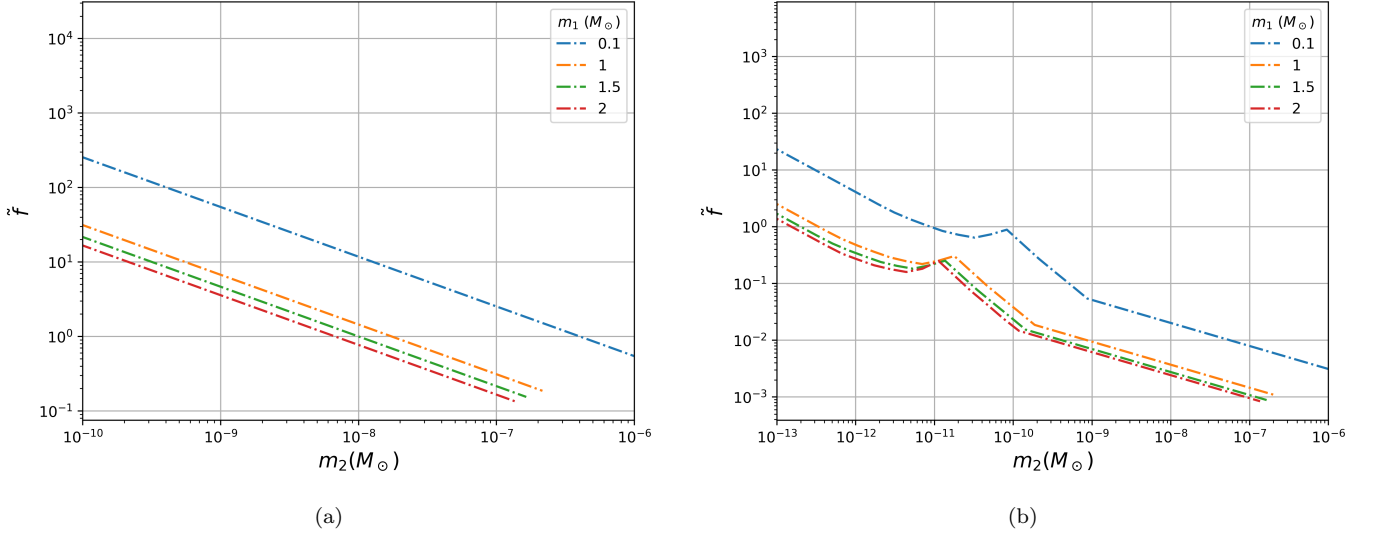


FIG. 10. NEMO sensitivity between 1000 and 2500 Hz. The curves extend to different values of  $m_2$  because we have fixed the chirp mass range to be  $[10^{-10}, 10^{-4}]M_\odot$ , which, for different choices of  $m_1$ , results in different values for  $m_2$ . Left: CW semi-coherent sensitivity. Right: matched-filter sensitivity. In the orange, green and red curves, we observe two “kinks”: one at  $\sim 5 \times 10^{-12}M_\odot$ , and another at  $\sim 10^{-10}M_\odot$ . The first kink occurs when the signal duration no longer exceeds the observation time, i.e. it becomes more “transient-like”. In practical terms, summing the contributions to the rate densities from different frequencies, outlined in Section IV, does not produce as competitive constraints as simply calculating the rate density in the Euclidean way (Eq. (26)). The second kink separates two regimes of different slopes, and results because, for sufficiently light  $m_2$ ,  $d_{\max}$  occurs at a frequency between  $[f_{\min}, f_{\max}]$ . This happens because signals with these frequencies, in the span of  $T_{\text{obs}}$ , would actually spin out of the  $[f_{\min}, f_{\max}]$  band analyzed. Thus, we limit the frequency that we allow to signal to spin up to  $f_{\max}$ , which corresponds to them lasting shorter than  $T_{\text{obs}}$ . As  $m_2$  increases, the frequency that maximizes  $d(f)$  shifts to lower and lower frequencies. When that frequency falls below 1000 Hz, we observe the second kink, and the slope changes, since after the second kink, the maximum distance reached is always obtained by analyzing the full frequency range.

of the results from O3 show in Fig. 6. Here, we evaluate how  $\delta f$  could affect the sensitivity of the search. We note, however, that we consider a very simplified case in which we have a flat noise power spectral density, in order to arrive at a semi-analytical expression for the detectable space-time volume  $\langle VT \rangle$ , which then allows us to constrain the rate density and  $\tilde{f}$ .

We know that  $\langle VT \rangle$  depends on  $d_{\max}^3$  and  $T$ :

$$\langle VT \rangle = \frac{4}{3}\pi d(f)^3 T. \quad (\text{B1})$$

and we will work in the small  $\delta f$  limit, that is  $\delta f \ll f$ . We can write an abbreviated form of Eq. (5):

$$\begin{aligned} d(f) &\propto f^{2/3} \\ T &\propto \delta f f^{-11/3} \\ V &\propto d(f)^3 \propto f^2 \\ \langle VT \rangle &\propto \delta f f^{-5/3} \end{aligned} \quad (\text{B2})$$

We thus see how  $\langle VT \rangle$  depends on  $f$  and  $\delta f$ . Now, we note that when we use Eq. (14), we are actually summing the distances at particular frequencies in steps of  $\delta f$ , since, typically, the upper limits on  $h_{0,\min}$  are given

in steps of  $\delta f$ . In mathematical terms, this corresponds to a summation of the form:

$$\begin{aligned} \langle VT \rangle_{\text{tot}} &= \sum \langle VT \rangle \propto \delta f \sum_{n=0}^N f_n^{-5/3} \\ &\propto \delta f (f_{\min}^{-5/3} + (f_{\min} + \delta f)^{-5/3} + (f_{\min} + 2\delta f)^{-5/3} \\ &\quad + \dots) \end{aligned} \quad (\text{B3})$$

$$\propto \delta f f_{\min}^{-5/3} \sum_{n=0}^N \left(1 + n \frac{\delta f}{f_{\min}}\right)^{-5/3} \quad (\text{B4})$$

where  $N = (f_{\max} - f_{\min})/\delta f$  is the number of frequencies that we sum. As noted before, for simplicity, we have set  $S_n(f) = \text{constant}$ , but its variation with frequency will affect the sum in practice, and could be parameterized as “weights” that affect each term in the sum.

This particular sum can in fact be represented in terms of Hurwitz zeta functions:

$$\sum_{n=0}^N (1 + nz)^{-5/3} = 1 + \frac{\zeta(\frac{5}{3}, 1 + \frac{1}{z}) - \zeta(\frac{5}{3}, N + \frac{1}{z} + 1)}{z^{5/3}} \quad (\text{B5})$$

where  $z = \delta f / f_{\min}$ , and when applied to our case:

$$\langle VT \rangle_{\text{tot}} = \frac{5}{96\pi^{2/3}} \frac{1}{\Lambda^3} \left( \frac{T_{\text{FFFT}}^{1/2} T_{\text{obs}}^{1/2}}{S_n} \right)^{3/2} \left( \frac{GM}{c^{21/10}} \right)^{10/3} \delta f^{-2/3} \left\{ \left( \frac{\delta f}{f_{\min}} \right)^{5/3} + \left[ \zeta \left( \frac{5}{3}, 1 + \frac{f_{\min}}{\delta f} \right) - \zeta \left( \frac{5}{3}, N + \frac{f_{\min}}{\delta f} + 1 \right) \right] \right\} \quad (\text{B6})$$

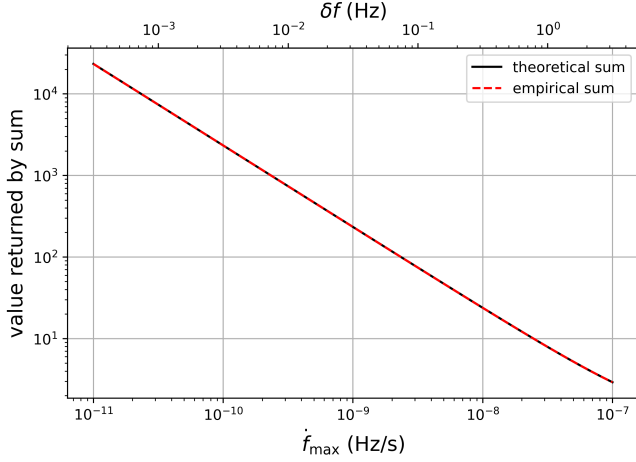


FIG. 11. Comparison of Eq. (B5) and Eq. (14), where in Eq. (14), we have neglected the prefactors and divided out the common frequency  $f_{\min}^{-5/3}$ .

where we have dropped the  $f$  argument on  $S_n$  to indicate that we have considered a flat noise spectral density.

We will fix  $f_{\min} = 5$  Hz and  $f_{\max} = 2000$  Hz, and consider to what extent this formulation agrees with what we actually do in Eq. (14), and how  $\langle VT \rangle$  depends on  $\delta f$ . We show this comparison in Fig. 11, and conclude that our theoretical formulation matches with the empirical one.

We then compute the impact of  $\delta f$  on  $\tilde{f}$ :

$$\mathcal{R} \propto \langle VT \rangle_{\text{tot}}^{-1} \quad (\text{B7})$$

$$\tilde{f}^{53/37} \propto \langle VT \rangle_{\text{tot}}^{-1} \quad (\text{B8})$$

$$\tilde{f} \propto \langle VT \rangle_{\text{tot}}^{-37/53} \quad (\text{B9})$$

and show the ratio of  $\tilde{f}$  to  $\tilde{f}_{\min}$  in Fig. 12.

From Eq. (B6) and from Fig. 11, we see a quite complicated dependence on  $\delta f$ , and note that what we have just derived above is *theoretical*, assuming a fixed noise power spectral density. The real situation is more complicated, and we cannot find a closed-form expression for the sum, since, in the case of a varying power spectral density, the sum on the left-hand side in Eq. (B5) takes on frequency-dependent weights. Additionally, the theoretical formulation does not impose any restrictions on

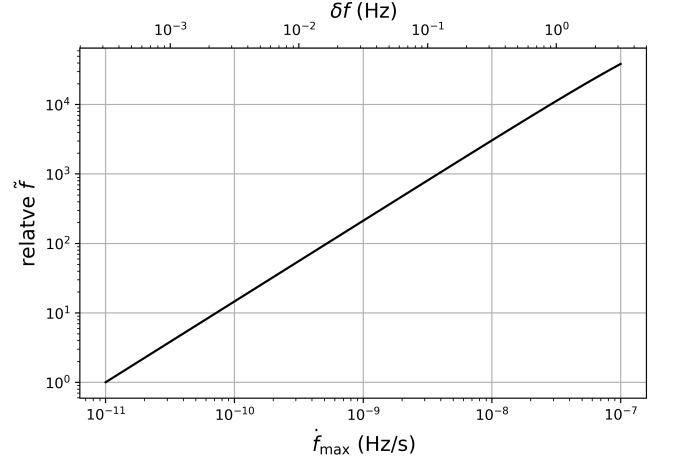


FIG. 12. The increase in the constraint  $\tilde{f}$  with respect to the minimum  $\tilde{f}$  attainable in this example with the smallest  $\delta f$  spacing. Note that this figure assumes a flat power spectral density and no restrictions on linearity or  $\dot{f}_{\max}$ . In practice, the relative  $\tilde{f}$  is much smaller.

linearity or on the maximum  $\dot{f}$  that a GW signal could take, both of which affect the constraint on  $\tilde{f}$ . However, our theoretical results highlight that there *is* a dependence on the spacing in frequency  $\delta f$  of the upper limits  $h_0(f)$ , which explains why, in Fig. 6, that changing  $\dot{f}_{\max}$  does not necessarily lead to better constraints on  $\tilde{f}$ .

## ACKNOWLEDGMENTS

This material is based upon work supported by NSF's LIGO Laboratory which is a major facility fully funded by the National Science Foundation

This research has made use of data, software and/or web tools obtained from the Gravitational Wave Open Science Center (<https://www.gw-openscience.org/>), a service of LIGO Laboratory, the LIGO Scientific Collaboration and the Virgo Collaboration. LIGO Laboratory and Advanced LIGO are funded by the United States National Science Foundation (NSF) as well as the Science and Technology Facilities Council (STFC) of the United Kingdom, the Max-Planck-Society (MPS), and

the State of Niedersachsen/Germany for support of the construction of Advanced LIGO and construction and operation of the GEO600 detector. Additional support for Advanced LIGO was provided by the Australian Research Council. Virgo is funded, through the European Gravitational Observatory (EGO), by the French Centre National de Recherche Scientifique (CNRS), the Italian

Istituto Nazionale della Fisica Nucleare (INFN) and the Dutch Nikhef, with contributions by institutions from Belgium, Germany, Greece, Hungary, Ireland, Japan, Monaco, Poland, Portugal, Spain.

We would like to thank all of the essential workers who put their health at risk during the COVID-19 pandemic, without whom we would not have been able to complete this work.

- 
- [1] S. Hawking, *Mon. Not. Roy. Astron. Soc.* **152**, 75 (1971).
- [2] G. F. Chapline, *Nature* **253**, 251 (1975).
- [3] J. Aasi, B. Abbott, R. Abbott, T. Abbott, M. Abernathy, K. Ackley, C. Adams, T. Adams, P. Addesso, R. Adhikari, *et al.*, *Classical and quantum gravity* **32**, 074001 (2015).
- [4] F. Acernese, M. Agathos, K. Agatsuma, D. Aisa, N. Allemandou, A. Allocca, J. Amarni, P. Astone, G. Balestri, G. Ballardín, *et al.*, *Classical and Quantum Gravity* **32**, 024001 (2014).
- [5] B. Abbott *et al.* (LIGO Scientific Collaboration, Virgo), *Phys. Rev. Lett.* **116**, 061102 (2016), arXiv:1602.03837 [gr-qc].
- [6] B. Abbott *et al.* (LIGO Scientific Collaboration, Virgo), *Phys. Rev. X* **6**, 041015 (2016), [Erratum: *Phys. Rev. X* **8**, 039903 (2018)], arXiv:1606.04856 [gr-qc].
- [7] B. P. Abbott *et al.* (LIGO Scientific Collaboration, Virgo), *Phys. Rev. Lett.* **116**, 241103 (2016), arXiv:1606.04855 [gr-qc].
- [8] B. P. Abbott *et al.* (LIGO Scientific Collaboration, Virgo), *Phys. Rev. Lett.* **118**, 221101 (2017), [Erratum: *Phys. Rev. Lett.* **121**, 129901 (2018)], arXiv:1706.01812 [gr-qc].
- [9] B. P. Abbott *et al.* (LVC), *Phys. Rev. Lett.* **119**, 141101 (2017), arXiv:1709.09660 [gr-qc].
- [10] B. P. Abbott *et al.* (LIGO Scientific Collaboration, Virgo), *Astrophys. J.* **851**, L35 (2017), arXiv:1711.05578 [astro-ph.HE].
- [11] B. P. Abbott *et al.* (LIGO Scientific Collaboration, Virgo), *Phys. Rev.* **X9**, 031040 (2019), arXiv:1811.12907 [astro-ph.HE].
- [12] R. Abbott *et al.* (LIGO Scientific Collaboration, Virgo), *Phys. Rev. D* **102**, 043015 (2020), arXiv:2004.08342 [astro-ph.HE].
- [13] B. Abbott *et al.* (LIGO Scientific Collaboration, Virgo), *Astrophys. J. Lett.* **892**, L3 (2020), arXiv:2001.01761 [astro-ph.HE].
- [14] R. Abbott *et al.* (LIGO Scientific Collaboration, Virgo), *Astrophys. J.* **896**, L44 (2020), arXiv:2006.12611 [astro-ph.HE].
- [15] R. Abbott *et al.* (LIGO Scientific Collaboration, Virgo), *Phys. Rev. Lett.* **125**, 101102 (2020), arXiv:2009.01075 [gr-qc].
- [16] R. Abbott *et al.* (LIGO Scientific Collaboration, Virgo), *Astrophys. J.* **900**, L13 (2020), arXiv:2009.01190 [astro-ph.HE].
- [17] C. Alcock *et al.* (MACHO), *Astrophys. J.* **486**, 697 (1997), arXiv:astro-ph/9606165.
- [18] A. Drlica-Wagner *et al.* (DES), *Astrophys. J.* **813**, 109 (2015), arXiv:1508.03622 [astro-ph.GA].
- [19] J. S. Bullock and M. Boylan-Kolchin, *Ann. Rev. Astron. Astrophys.* **55**, 343 (2017), arXiv:1707.04256 [astro-ph.CO].
- [20] B. Carr, S. Clesse, J. García-Bellido, and F. Kühnel, *Phys. Dark Univ.* **31**, 100755 (2021), arXiv:1906.08217 [astro-ph.CO].
- [21] P. Villanueva-Domingo, O. Mena, and S. Palomares-Ruiz, *Front. Astron. Space Sci.* **8**, 87 (2021), arXiv:2103.12087 [astro-ph.CO].
- [22] A. M. Green and B. J. Kavanagh, *J. Phys. G* **48**, 043001 (2021), arXiv:2007.10722 [astro-ph.CO].
- [23] A. Ulmer and J. Goodman, *Astrophys. J.* **442**, 67 (1995), arXiv:astro-ph/9406042.
- [24] H. Aihara *et al.*, *Publ. Astron. Soc. Jap.* **70**, S4 (2018), arXiv:1704.05858 [astro-ph.IM].
- [25] H. Aihara *et al.*, *Publ. Astron. Soc. Jap.* **70**, S8 (2018), arXiv:1702.08449 [astro-ph.IM].
- [26] H. Niikura *et al.*, *Nature Astron.* **3**, 524 (2019), arXiv:1701.02151 [astro-ph.CO].
- [27] N. Smyth, S. Profumo, S. English, T. Jeltema, K. McKinnon, and P. Guhathakurta, *Phys. Rev. D* **101**, 063005 (2020), arXiv:1910.01285 [astro-ph.CO].
- [28] A. Gould, *Astrophysical Journal, Part 2-Letters (ISSN 0004-637X)*, vol. 386, Feb. 10, 1992, p. L5-L7. **386**, L5 (1992).
- [29] S. Davidson and T. Schwetz, *Phys. Rev. D* **93**, 123509 (2016), arXiv:1603.04249 [astro-ph.CO].
- [30] A. Barnacka, J. F. Glicenstein, and R. Moderski, *Phys. Rev. D* **86**, 043001 (2012), arXiv:1204.2056 [astro-ph.CO].
- [31] A. Katz, J. Kopp, S. Sibiryakov, and W. Xue, *JCAP* **12**, 005 (2018), arXiv:1807.11495 [astro-ph.CO].
- [32] R. C. Hickox, R. Narayan, and T. R. Kallman, *Astrophys. J.* **614**, 881 (2004), arXiv:astro-ph/0407115.
- [33] A. M. Levine, H. Bradt, W. Cui, J. G. Jernigan, E. H. Morgan, R. Remillard, R. E. Shirey, and D. A. Smith, *Astrophys. J. Lett.* **469**, L33 (1996), arXiv:astro-ph/9608109.
- [34] S.-N. Zhang *et al.* (eXTP), *Sci. China Phys. Mech. Astron.* **62**, 29502 (2019), arXiv:1812.04020 [astro-ph.IM].
- [35] Y. Bai and N. Orlofsky, *Phys. Rev. D* **99**, 123019 (2019), arXiv:1812.01427 [astro-ph.HE].
- [36] S. Babak, J. Gair, A. Sesana, E. Barausse, C. F. Sopuerta, C. P. L. Berry, E. Berti, P. Amaro-Seoane, A. Petiteau, and A. Klein, *Phys. Rev. D* **95**, 103012 (2017), arXiv:1703.09722 [gr-qc].
- [37] H.-K. Guo and A. Miller, (2022), arXiv:2205.10359 [astro-ph.IM].
- [38] M. Sieniawska and M. Beijger, *Universe* **5**, 217 (2019), arXiv:1909.12600 [astro-ph.HE].
- [39] R. Tenorio, D. Keitel, and A. M. Sintes, *Universe* **7**, 474 (2021), arXiv:2111.12575 [gr-qc].

- [40] K. Riles, *Living Rev. Rel.* **26**, 3 (2023), arXiv:2206.06447 [astro-ph.HE].
- [41] O. J. Piccinni, *Galaxies* **10**, 72 (2022), arXiv:2202.01088 [gr-qc].
- [42] A. L. Miller (LIGO Scientific Collaboration, Virgo, KAGRA), in *57th Rencontres de Moriond on Gravitation* (2023) arXiv:2305.15185 [gr-qc].
- [43] K. Wette, *Astropart. Phys.* **153**, 102880 (2023), arXiv:2305.07106 [gr-qc].
- [44] A. L. Miller, N. Aggarwal, S. Clesse, and F. De Lillo, *Phys. Rev. D* **105**, 062008 (2022), arXiv:2110.06188 [gr-qc].
- [45] R. Abbott *et al.* (LIGO Scientific Collaboration, Virgo, KAGRA), *Phys. Rev. D* **106**, 102008 (2022), arXiv:2201.00697 [gr-qc].
- [46] M. Maggiore, *Gravitational Waves: Volume 1: Theory and Experiments*, Vol. 1 (Oxford University Press, 2008).
- [47] B. Steltner, M. A. Papa, H. B. Eggenstein, R. Prix, M. Bensch, B. Allen, and B. Machenschalk, *Astrophys. J.* **952**, 55 (2023), arXiv:2303.04109 [gr-qc].
- [48] R. Prix, in *Neutron Stars and Pulsars*, ASSL, Vol. 357, edited by W. Becker (Springer Berlin Heidelberg, 2009) Chap. 24, pp. 651–685.
- [49] V. Dergachev and M. A. Papa, *Phys. Rev. D* **109**, 022007 (2024), arXiv:2401.13173 [gr-qc].
- [50] A. L. Miller *et al.*, *Phys. Rev. D* **103**, 103002 (2021), arXiv:2010.01925 [astro-ph.IM].
- [51] R. Abbott *et al.* (LIGO Scientific Collaboration, Virgo, KAGRA), *Phys. Rev. D* **105**, 063030 (2022), arXiv:2105.13085 [astro-ph.CO].
- [52] A. L. Miller, N. Aggarwal, S. Clesse, F. De Lillo, S. Sachdev, P. Astone, C. Palomba, O. J. Piccinni, and L. Pierini, *Phys. Rev. Lett.* **133**, 111401 (2024), arXiv:2402.19468 [gr-qc].
- [53] A. L. Miller, N. Aggarwal, S. Clesse, F. De Lillo, S. Sachdev, P. Astone, C. Palomba, O. J. Piccinni, and L. Pierini, In press, *Phys. Rev. D.* (2024), arXiv:2407.17052 [astro-ph.IM].
- [54] A. L. Miller, (2024), arXiv:2404.11601 [gr-qc].
- [55] S. Bhattacharya, A. L. Miller, and A. Ray, *Phys. Rev. D* **110**, 043006 (2024), arXiv:2403.13886 [hep-ph].
- [56] P. Astone, A. Colla, S. D’Antonio, S. Frasca, and C. Palomba, *Physical Review D* **90**, 042002 (2014).
- [57] M. Maggiore *et al.*, *JCAP* **03**, 050 (2020), arXiv:1912.02622 [astro-ph.CO].
- [58] M. Branchesi *et al.*, *JCAP* **07**, 068 (2023), arXiv:2303.15923 [gr-qc].
- [59] A. L. Miller, S. Clesse, F. De Lillo, G. Bruno, A. Depasse, and A. Tanasijczuk, *Phys. Dark Univ.* **32**, 100836 (2021), arXiv:2012.12983 [astro-ph.HE].
- [60] M. Andrés-Carcasona, O. J. Piccinni, M. Martínez, and L.-M. Mir, *PoS EPS-HEP2023*, 067 (2023).
- [61] G. Alestas, G. Morras, T. S. Yamamoto, J. Garcia-Bellido, S. Kuroyanagi, and S. Nesseris, *Phys. Rev. D* **109**, 123516 (2024), arXiv:2401.02314 [astro-ph.CO].
- [62] I. Kowalska, T. Bulik, K. Belczynski, M. Dominik, and D. Gondek-Rosinska, *Astron. Astrophys.* **527**, A70 (2011), arXiv:1010.0511 [astro-ph.CO].
- [63] J. Samsing, M. MacLeod, and E. Ramirez-Ruiz, *Astrophys. J.* **784**, 71 (2014), arXiv:1308.2964 [astro-ph.HE].
- [64] J. Samsing, *Phys. Rev. D* **97**, 103014 (2018), arXiv:1711.07452 [astro-ph.HE].
- [65] J. N. Arredondo, A. Klein, and N. Yunes, *Phys. Rev. D* **110**, 044044 (2024), arXiv:2402.06804 [gr-qc].
- [66] R. Abbott *et al.* (KAGRA, LIGO Scientific, VIRGO), *Phys. Rev. D* **106**, 042003 (2022), arXiv:2204.04523 [astro-ph.HE].
- [67] A. Miller *et al.*, *Phys. Rev. D* **98**, 102004 (2018), arXiv:1810.09784 [astro-ph.IM].
- [68] N. Aggarwal *et al.*, *Living Rev. Rel.* **24**, 4 (2021), arXiv:2011.12414 [gr-qc].